J. Fluid Mech. (2014), *vol.* 755, *pp.* 654–671.
doi:10.1017/jfm.2014.307

Helicity in the Ekman boundary layer

Enrico Deusebio[1,2,†] **and Erik Lindborg**[2]

[1]Department of Applied Mathematics and Theoretical Physics, Centre for Mathematical Sciences, Cambridge CB3 0WA, UK

[2]Linné Flow Centre, Department of Mechanics, Royal Institute of Technology (KTH), SE-10044 Stockholm, Sweden

(Received 17 October 2013; revised 22 May 2014; accepted 26 May 2014; first published online 26 August 2014)

Helicity, which is defined as the scalar product of velocity and vorticity, $\mathcal{H} = \boldsymbol{u} \cdot \boldsymbol{\omega}$, is an inviscidly conserved quantity in a barotropic fluid. Mean helicity is zero in flows that are parity invariant. System rotation breaks parity invariance and has therefore the potential of giving rise to non-zero mean helicity. In this paper we study the helicity dynamics in the incompressible Ekman boundary layer. Evolution equations for the mean field helicity and the mean turbulent helicity are derived and it is shown that pressure flux injects helicity at a rate $2\Omega G^2$ over the total depth of the Ekman layer, where G is the geostrophic wind far from the wall and $\boldsymbol{\Omega} = \Omega \boldsymbol{e}_y$ is the rotation vector and $\boldsymbol{e}_y$ is the wall-normal unit vector. Thus right-handed/left-handed helicity will be injected if Ω is positive/negative. We also show that in the uppermost part of the boundary layer there is a net helicity injection with opposite sign as compared with the totally integrated injection. Isotropic relations for the helicity dissipation and the helicity spectrum are derived and it is shown that it is sufficient to measure two transverse velocity components and use Taylor's hypothesis in the mean flow direction in order to measure the isotropic helicity spectrum. We compare the theoretical predictions with a direct numerical simulation of an Ekman boundary layer and confirm that there is a preference for right-handed helicity in the lower part of the Ekman layer and left-handed helicity in the uppermost part when $\Omega > 0$. In the logarithmic range, the helicity dissipation conforms to isotropic relations. On the other hand, spectra show significant departures from isotropic conditions, suggesting that the Reynolds number considered in the study is not sufficiently large for isotropy to be valid in a wide range of scales. Our analytical and numerical results strongly suggest that there is a turbulent helicity cascade of right-handed helicity in the logarithmic range of the atmospheric boundary layer when $\Omega > 0$, consistent with recent measurements by Koprov, Koprov, Ponomarev & Chkhetiani (*Dokl. Phys.*, vol. 50, 2005, pp. 419–422). The isotropic relations which are derived may facilitate future measurements of the helicity spectrum in the atmospheric boundary layer as well as in controlled wind tunnel experiments.

Key words: atmospheric flows, rotating turbulence, turbulence theory

† Email address for correspondence: deusebio@mech.kth.se

1. Introduction

Inviscidly conserved quantities have a particular importance in fluid dynamics, especially in the context of turbulence. Prime examples are kinetic energy and in two-dimensions enstrophy, defined as half the square of vorticity. Moffatt (1969) showed that helicity, $\mathcal{H} = \boldsymbol{\omega} \cdot \boldsymbol{u}$, is such a conserved quantity in a barotropic fluid. However, unlike energy and enstrophy, helicity is not positive definite. This is the reason why the conservation of two separate quadratic invariants, energy and helicity, does not lead to an inverse energy cascade in three-dimensional turbulence (Biferale 2003). Recent numerical simulations have shown that if only nonlinear interactions involving only positive or negative helical modes are retained an inverse cascade of energy and a forward cascade of helicity develop (Biferale, Musacchio & Toschi 2012), as in 2D turbulence where there is an inverse energy cascade and a forward enstrophy cascade (Kraichnan 1967). On the other hand, numerical simulations of the full three-dimensional Navier–Stokes equations (Borue & Orszag 1997; Chen *et al.* 2003*b*; Mininni, Alexakis & Pouquet 2006) have shown the existence of a joint energy and helicity cascade towards small scales. The energy spectrum is found to scale as $E(k) \sim \varepsilon^{2/3} k^{-5/3}$ and the helicity spectrum as $H(k) \sim \chi_h \varepsilon^{-1/3} k^{-5/3}$, in agreement with theoretical predictions (Brissaud *et al.* 1973). Here, ε and χ_h are the energy and helicity turbulent dissipation, respectively. Numerical simulations of homogeneous turbulence also show that the helicity cascade towards small scales is robust and is maintained also in the presence of a system rotation (Mininni & Pouquet 2009). In meteorology, helicity has been used to predict the development of tornados (Thompson 2005) and such phenomena are commonly presented as examples of highly helical flows (Tsinober & Levich 1983; Lilly 1986; Moffatt & Tsinober 1992).

Mean helicity is zero in flows that are parity invariant. System rotation breaks parity invariance and may therefore lead to a non-zero mean helicity, a fact that has been pointed out in a number of studies (Brissaud *et al.* 1973; Etling 1985). It has also been pointed out that the laminar Ekman layer is helical (Zhemin & Rongsheng 1994), with a preference for right-handed helicity in the lower part of the Ekman layer and left-handed helicity in the uppermost part. There have been some attempts to measure the helicity spectrum in the laboratory using hot wires (Kholmyansky *et al.* 1991). However, it has proven extremely difficult to measure different components of the vorticity and the velocity in a single point. Quite recently, however, the helicity spectrum has been measured in an atmospheric boundary layer using acoustic Doppler anemometry (Koprov *et al.* 2005). A special technique was used to retrieve different components of vorticity from the acoustic signal, and found that the helicity spectrum displayed a $k^{-5/3}$ range over a decade of wavenumbers. Despite these efforts, it has not been clarified by what mechanism system rotation may give rise to a non-zero mean helicity, and why mean helicity should either be right- or left-handed.

As shown by Moffatt (1969), mean helicity is conserved in a control volume containing an inviscid barotropic fluid, where the normal component of vorticity is zero at the boundaries. This is true also in the presence of system rotation and conservative forces, such as gravity. Consider a standard square box control volume in a barotropic boundary layer, with one side coinciding with the wall and the opposing side very far from the wall. In such a volume mean helicity can only be generated by viscous mechanisms or by a flux through the lateral boundaries. We will show that it is by a pressure flux through the lateral boundaries that mean helicity is generated in the incompressible Ekman boundary layer and that viscosity mainly acts as to destroy the mean helicity which is generated. This is analogous to the injection

of mean kinetic energy generated by pressure work, $-\int \boldsymbol{n}\cdot(p\boldsymbol{u})\,\mathrm{d}S$, acting at the lateral surfaces of a control volume, and dissipated by viscosity. Here, $\boldsymbol{n}$ is the unit vector normal to the control volume surface. In a similar way, the helicity equation contains two terms, the net helicity gain, $-\int \boldsymbol{n}\cdot(p\boldsymbol{\omega})\,\mathrm{d}S$, by pressure flux acting at the lateral surfaces and the helicity loss due to viscous destruction. In a non-rotating boundary layer the mean vorticity is perpendicular to the pressure gradient, resulting in a zero net helicity gain. In the Ekman boundary layer, this is not the case and net helicity will therefore be injected into a control volume in which the boundary layer is statistically stationary. The injection process takes place at large scales, comparable to the turbulent integral length scale, and since helicity is an inviscidly conserved quantity, it can only be dissipated by viscosity which is acting at the very smallest scale of turbulence, the Kolmogorov scale. Thus, there must exist a transfer of helicity from large to small scales, that is a helicity cascade.

The paper is organised as follows. In § 2 we derive the relevant dynamical equations for the mean and turbulent helicity and apply them to an Ekman boundary layer. We also derive some isotropic relations which may facilitate a future measurement of the helicity spectrum and the helicity dissipation. In § 3 we present a data analysis from a recent direct numerical simulation (DNS) of the neutrally stratified Ekman boundary layer and interpret the results in the light of the analytical results. In § 4 we end the paper with conclusions.

2. Theory

2.1. *Basic equations*

We start by deriving the equations for the total helicity budget. In nearly neutrally stratified conditions, the dynamics of the atmospheric boundary layer can be described, at first approximation, by means of the three-dimensional incompressible Navier–Stokes equations in a rotating reference frame (see e.g. Vallis 2006; Spalart, Coleman & Johnstone 2009),

$$\frac{\partial \boldsymbol{u}}{\partial t}+\boldsymbol{u}\cdot\boldsymbol{\nabla}\boldsymbol{u}=-\frac{\boldsymbol{\nabla}p}{\rho_0}-2\boldsymbol{\Omega}\times\boldsymbol{u}+\nu\nabla^2\boldsymbol{u}, \tag{2.1a}$$

$$\boldsymbol{\nabla}\cdot\boldsymbol{u}=0. \tag{2.1b}$$

Here, $\boldsymbol{u}=(u,v,w)$ is the velocity vector in the right-handed Cartesian system (x,y,z) with x and z being the horizontal coordinates and y the vertical coordinate, p is the pressure, ν is the kinematic viscosity and $\boldsymbol{\Omega}$ is the rotation vector, which is assumed to be vertical. The convention of using y rather than z as the vertical coordinate is standard in DNS of boundary layers, including Ekman boundary layers (see e.g. Shingai & Kawamura 2004). In geophysical applications, the f-plane approximation is usually made, by considering a system subjected to only a vertical rotation rate of intensity $\Omega\sin\Theta$, where Θ is the latitude and Ω is the rotation rate of the Earth.

We divide the total mean helicity $\overline{\mathcal{H}}$ into a mean field contribution and a turbulent contribution,

$$\overline{\mathcal{H}}=\overline{u_i\omega_i}=H+h, \tag{2.2}$$

where $H\equiv\overline{u}_i\overline{\omega}_i$, $h\equiv\overline{u_i'\omega_i'}$ and $\overline{\cdot}$ stands for an ensemble average and the prime, $'$, denotes the deviation from the mean. We say that the helicity is right-handed/left-handed if it positive/negative when a right-handed coordinate system is used in the calculation of the vorticity.

The evolution equations for the mean field helicity H and the turbulent helicity h are derived from the system (2.1) in a similar way as done for the kinetic energy budget equations. The equations can be written in compact from as

$$\frac{\mathrm{d}H}{\mathrm{d}t} = -P - \chi_H + T + I + R, \tag{2.3}$$

$$\frac{\mathrm{d}h}{\mathrm{d}t} = P - \chi_h + t + i + r. \tag{2.4}$$

The turbulent helicity production term,

$$P = -\overline{u_i' u_j'}\frac{\partial \overline{\omega}_i}{\partial x_j} - \left(\overline{\omega_i' u_j'} - \overline{\omega_j' u_i'}\right)\frac{\partial \overline{u}_i}{\partial x_j}, \tag{2.5}$$

converts helicity between the mean and the turbulent fields. Here χ_H and χ_h are the mean and turbulent helicity dissipation, respectively, given by

$$\chi_H = 2\nu \frac{\partial \overline{u}_i}{\partial x_k}\frac{\partial \overline{\omega}_i}{\partial x_k} \quad \text{and} \quad \chi_h = 2\nu \overline{\frac{\partial u_i'}{\partial x_k}\frac{\partial \omega_i'}{\partial x_k}}. \tag{2.6a,b}$$

Here T and t are transport terms,

$$T = -\frac{\partial}{\partial x_j}\left\{\overline{u}_j H - \frac{1}{2}\overline{\omega}_j \overline{u}_i^2 + \overline{\omega}_i \overline{u_i' u_j'} + \overline{u_i}\overline{\omega_i' u_j' - \omega_j' u_i'} - \nu \frac{\partial H}{\partial x_j}\right\}, \tag{2.7}$$

$$t = -\frac{\partial}{\partial x_j}\left\{\overline{u}_j h - \frac{1}{2}\overline{\omega}_j \overline{u_i'^2} + \overline{u_i' u_j' \omega_i'} - \frac{1}{2}\overline{\omega_j' u_i'^2} - \nu \frac{\partial h}{\partial x_j}\right\}. \tag{2.8}$$

Here I and i are the helicity transport terms arising from the pressure term. These are given by

$$I = -\frac{\partial \overline{p}}{\partial x}\overline{\omega}_x - \frac{\partial \overline{p}}{\partial z}\overline{\omega}_z \quad \text{and} \quad i = -\frac{\partial}{\partial x_i}\overline{p'\omega_i'}. \tag{2.9a,b}$$

R and r are the Coriolis transport terms, defined as

$$R = 2\Omega_i \frac{\partial}{\partial x_k}\overline{u}_k \overline{u}_i \quad \text{and} \quad r = 2\Omega_i \frac{\partial}{\partial x_k}\overline{u_k' u_i'}. \tag{2.10a,b}$$

The latter terms are the only terms that are not parity invariant and explicitly include rotation. Thus, during spin-up from a parity invariant initial state with no helicity, these terms are the only ones that can set up a gradient of helicity in the vertical direction. Assuming homogeneity in the horizontal direction, i.e.

$$\partial/\partial x\,\overline{\cdot} = \partial/\partial z\,\overline{\cdot} = 0, \tag{2.11}$$

we find that the Coriolis term has the form $2\Omega\,\partial v^2/\partial y$. Thus, in a bottom boundary layer during spin-up this term moves helicity from the outer part to the inner part of the boundary layer.

We now restrict ourselves to a statistically stationary state where the Ekman layer is statistically homogeneous in the horizontal directions. In this case R is equal to zero, while T, t, i and r reduce to

$$T = -\frac{\mathrm{d}}{\mathrm{d}y}\left\{\overline{\omega}_i \overline{u_i' v'} + \overline{u_i}\overline{\omega_i' v' - \omega_y' u_i'} - \nu \frac{\mathrm{d}H}{\mathrm{d}y}\right\}, \tag{2.12}$$

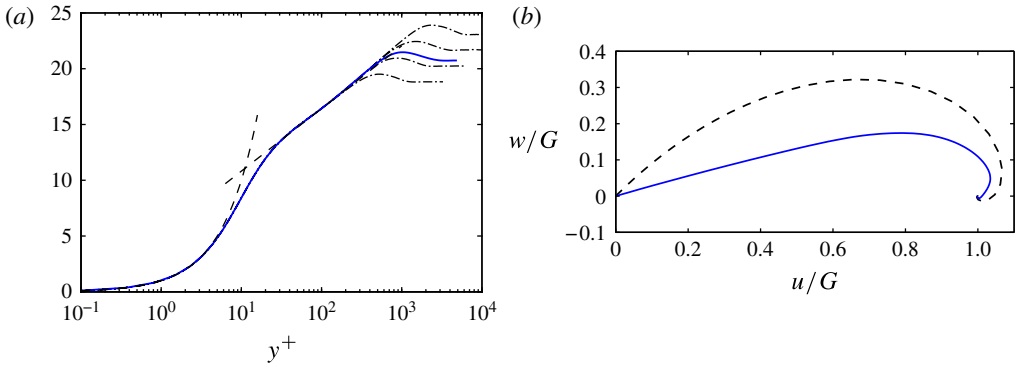

FIGURE 1. (Colour online) (*a*) Total horizontal wind $\sqrt{\overline{u}^2 + \overline{w}^2}/u_\tau$. The vertical direction y is scaled by the viscous scale, i.e. $y^+ = y/l^+ = yu_\tau/\nu$. Thin lines represent the law of the wall $\overline{u}^+ = y^+$ and the logarithmic region $\overline{u}^+ = 1/0.41 \log y^+ + 5.5$. $-\cdot-$ (thin) (Spalart *et al.* 2009) at $Re = 1000, 1414, 2000, 2828$. (*b*) Ekman spiral for - - - - a laminar Ekman boundary layer and —— a turbulent Ekman boundary layer.

$$t = -\frac{\mathrm{d}}{\mathrm{d}y}\left\{\overline{v'u_i'\omega_i'} - \frac{1}{2}\overline{\omega_y' u_i'^2} - \nu\frac{\mathrm{d}h}{\mathrm{d}y}\right\}, \tag{2.13}$$

$$i = -\frac{\mathrm{d}}{\mathrm{d}y}\overline{p'\omega_y'}, \tag{2.14}$$

$$r = 2\Omega\frac{\mathrm{d}}{\mathrm{d}y}\overline{v'^2}. \tag{2.15}$$

The term I requires special attention. As we pointed out in § 1, it is the only source term, accounting for a helicity flux into a control volume through the lateral boundaries. The velocity vector far from the wall, $\boldsymbol{u}_\infty = \boldsymbol{G}$, is in geostrophic balance, that is $\boldsymbol{\nabla}\overline{p} = -2\boldsymbol{\Omega} \times \boldsymbol{G}$. The injection of helicity integrated between two heights, y_1 and y_2, is thus given by

$$\int_{y_1}^{y_2} I\,\mathrm{d}y = -\int_{y_1}^{y_2} \boldsymbol{\nabla}\overline{p}\cdot\overline{\boldsymbol{\omega}}\,\mathrm{d}y = 2\Omega\int_{y_1}^{y_2} \boldsymbol{G}\cdot\frac{\partial\overline{\boldsymbol{u}}}{\partial y}\,\mathrm{d}y = 2\Omega\boldsymbol{G}\cdot(\overline{\boldsymbol{u}}_2 - \overline{\boldsymbol{u}}_1), \tag{2.16}$$

where $\overline{\boldsymbol{u}}_1$ and $\overline{\boldsymbol{u}}_2$ are the mean velocity vectors at heights y_1 and y_2, respectively. From (2.16), it is readily shown that the helicity injection integrated over the total depth of the Ekman layer is equal to $2\Omega G^2$. This shows that the quantity $\mathcal{H}\boldsymbol{e}_y \cdot \Omega$ is generally positive in the Ekman boundary layer. Thus, if Ω is positive/negative, right-handed/left-handed helicity will be injected. However, as seen in figure 1(*b*), in the upper part of the Ekman layer there is a point where the wind component parallel to the geostrophic wind has a maximum and is larger than G. Integrating I between this point and infinity we thus find that the helicity injection has opposite sign in the uppermost part of the Ekman layer as compared with the totally integrated injection.

For an Ekman boundary layer in a stationary state, there is a balance between total dissipation, $\chi = \chi_H + \chi_h$, and net injection, that is

$$\int_0^\infty \chi\,\mathrm{d}y = 2\Omega G^2. \tag{2.17}$$

In the laminar case, the injection of helicity is entirely balanced by the mean field helicity dissipation, χ_H. In the turbulent case this is not true and χ_h has a non-negligible contribution. In the logarithmic range, the mean field helicity dissipation can be estimated as $\chi_H \sim \nu u_\tau^2/\delta^3 \sim \nu\Omega^3/u_\tau$, where u_τ is the friction velocity and $\delta \sim u_\tau/\Omega$ is the boundary-layer thickness. Since the total integrated injection rate of helicity is $2\,\Omega G^2$, in the logarithmic range we can therefore estimate the helicity injection rate as $\Omega G^2/\delta \sim \Omega^2 G^2/u_\tau$. The ratio, χ_H/χ_h, between the mean field dissipation and the turbulent dissipation can thus be estimated as $\nu\Omega/G^2 = Re^{-2}$. Thus, virtually all the injected helicity will be dissipated by turbulent motions if $Re = G/\sqrt{\nu\Omega}$ is sufficiently large and $\chi_h = \chi$ at a large degree of accuracy. The general helicity budget in a control volume covering a section of a stationary Ekman boundary layer will thus be as follows. Right-handed mean field helicity is generated by the pressure flux I. Mean field helicity is then transferred to turbulent helicity through the production term P. The turbulent helicity undergoes a cascade in which it is successively transferred to smaller and smaller scales. Finally, helicity is dissipated by viscosity at the Kolmogorov scale.

2.2. *Isotropic relations*

The spectrum of helicity can be obtained by measuring the two-point correlation

$$\Phi(\boldsymbol{x}, \boldsymbol{r}) = \langle u_i(\boldsymbol{x})\omega_i(\boldsymbol{x}+\boldsymbol{r})\rangle, \tag{2.18}$$

where in this section we omit the primes for denoting the fluctuating parts of velocity and vorticity. According to Moffatt (1981), 'a first step' towards such a measurement would be a measurement of a correlation such as

$$\xi^{-1}(u(0,0,0)[w(r,\xi,0) - w(r,-\xi,0)]). \tag{2.19}$$

The two-point correlation (2.19) is a function of two coordinates of the separation vector. Therefore, a measurement of such a correlation cannot be performed by measuring two velocity components in a single point and using Taylor's hypothesis, by which the separation coordinate in the mean flow direction can be replaced by a time separation. Estimates based on (2.19) requires a spatial resolution for ξ of the order of the Kolmogorov scale, which in typical experimental and field situations is of the order of millimetres, thus making a measurement based on (2.19) very demanding. We will now show that, under the assumption of isotropy, it is possible to derive the helicity spectrum and the helicity dissipation from the more-accessible two-point velocity correlation

$$a(x) = \tfrac{1}{2}(\langle v(0,0,0)w(x,0,0)\rangle - \langle w(0,0,0)v(x,0,0)\rangle). \tag{2.20}$$

A measurement of $a(x)$ can be easily performed by simultaneously measuring the two transverse velocity components v and w in a single point and using Taylor's hypothesis in the mean flow direction.

Under the assumption of homogeneity, the two-point helicity correlation function (2.18) is independent of $\boldsymbol{x}$ and can be calculated from the two-point velocity correlation tensor as

$$\Phi(\boldsymbol{r}) = \epsilon_{ijk}\frac{\partial}{\partial r_j}\langle u_i u_k(\boldsymbol{r})\rangle, \tag{2.21}$$

where $u_k(\boldsymbol{r})$ is measured at a point with separation vector $\boldsymbol{r}$ relative to the point where u_i is measured. Under the assumption of rotational invariance (isotropy) Φ should be independent of the direction of $\boldsymbol{r}$ and thus be a function of $r = |\boldsymbol{r}|$. If rotational invariance, but not reflectional invariance, is imposed on the two-point velocity correlation tensor, it can be written in terms of three scalar functions

$$\langle u_i u_j(\boldsymbol{r})\rangle = n_i n_j f(r) + (\delta_{ij} - n_i n_j) g(r) + \epsilon_{ijk} n_k a(r), \tag{2.22}$$

where $\boldsymbol{n} = \boldsymbol{r}/r$ is the radial unit vector, f and g are the two standard longitudinal and transverse correlation functions (see e.g. Batchelor 1953), and $a(r)$ is the same function as defined in (2.20). The dynamical equation for $\Phi(r)$ and $a(r)$ have been derived and analysed by Chkhetiani (1996), Gomez, Politano & Pouquet (2000) and Kurien (2003). However, to the best of the authors' knowledge, the kinematical relations relating the helicity spectrum and the helicity dissipation to the measurable function $a(r)$ have not previously been derived. We do this by first using (2.21) and (2.22) to obtain

$$\Phi(r) = -\frac{2}{r^2}\frac{\mathrm{d}}{\mathrm{d}r}(r^2 a(r)). \tag{2.23}$$

Before proceeding with the analysis we should make a comment on the assumption of isotropy. Evidently, isotropy is a rather strong assumption to apply on the two-point velocity correlation since in the limit of zero correlation distance we obtain the Reynolds stress tensor, which is not isotropic in most experimental situations. However, we can relax the assumption of isotropy to be fulfilled when second- and higher-order derivatives of (2.23) are considered, which, as we will see in the following, is supported by the data analysis. For example, we can calculate the helicity dissipation if we have measured the variation of a at small separations. Since a is odd it can be expanded as

$$a(x) = a_1 x + a_3 x^3 + \mathcal{O}(x^5), \tag{2.24}$$

for small x. The helicity dissipation can now be calculated as

$$\chi_h = -2\nu\ (\nabla^2 \Phi(r))\big|_{r=0} = 4\nu\ \left(\nabla^2\left(\frac{1}{r^2}\frac{\partial}{\partial r}(r^2 a)\right)\right)\bigg|_{r=0} = 120\nu a_3, \tag{2.25}$$

where we recall that the Laplacian in spherical coordinates should be used here. Alternative expressions are

$$\chi_h = 20\nu\left\langle \frac{\partial^2 v}{\partial x^2}\frac{\partial w}{\partial x}\right\rangle = 20\nu\left\langle \frac{\partial^2 u}{\partial z^2}\frac{\partial v}{\partial z}\right\rangle = 20\nu\left\langle \frac{\partial^2 w}{\partial y^2}\frac{\partial u}{\partial y}\right\rangle. \tag{2.26}$$

The three-dimensional helicity spectrum can be defined by first introducing the three-dimensional Fourier transform

$$\widehat{\Phi}(\boldsymbol{k}) = \frac{1}{(2\pi)^3}\iiint \Phi(r)\exp(-\mathrm{i}\boldsymbol{k}\cdot\boldsymbol{r})\,\mathrm{d}^3 r. \tag{2.27}$$

Since Φ is a function of r, $\widehat{\Phi}$ is only a function of $k = |\boldsymbol{k}|$. The three-dimensional helicity spectrum is obtained by integration of $\widehat{\Phi}$ over a spherical shell as

$$H(k) = 4\pi k^2 \widehat{\Phi}(k). \tag{2.28}$$

The helicity spectrum can be related to the one-dimensional sine transform of $a(r)$,

$$F(k) = \frac{2}{\pi}\int_0^\infty a(r)\sin(kr)\,\mathrm{d}r. \tag{2.29}$$

Inserting (2.23) into (2.27), introducing spherical coordinates and integrating over the two angles, we find

$$H(k) = -\frac{4k}{\pi}\int_0^\infty a(r)[\sin(kr) - kr\cos(kr)]\,\mathrm{d}r = -2k\left[F(k) - k\frac{\mathrm{d}F}{\mathrm{d}k}\right]. \tag{2.30}$$

In a perfectly isotropic field, the expression (2.30) can be used to calculate the mean turbulent helicity as

$$h = \int_0^\infty H(k)\,\mathrm{d}k = -6a_1 = -6\int_0^\infty kF(k)\,\mathrm{d}k. \tag{2.31}$$

Since a Fourier decomposition of the flow field is easily carried out in both horizontal directions, it is natural to calculate the two-dimensional helicity spectrum, defined as

$$H_{2D}(k_h, y) = \int_{C(k_h)} \hat{\boldsymbol{u}}(k_x, k_z, y)\cdot\hat{\boldsymbol{\omega}}^*(k_x, k_z, y)\,\mathrm{d}C_k, \tag{2.32}$$

with

$$C(k_h) = \{(k_x, k_y, k_z)|k_h^2 = k_x^2 + k_z^2\}. \tag{2.33}$$

In the isotropic case the two-dimensional spectrum can be related to the three-dimensional spectrum (2.31) as

$$H_{2D}(k_h) = k_h\int_{k_h}^\infty \frac{H(k)}{k(k^2 - k_h^2)^{1/2}}\,\mathrm{d}k. \tag{2.34}$$

It should be emphasised that in a typical experimental context the mean helicity cannot be calculated as in (2.31), since isotropy can only be assumed for scales that are much smaller than the turbulent integral length scale. Nevertheless, since the smallest scales are fairly isotropic, the helicity dissipation can still be calculated as

$$\chi_h = 2\nu\int_0^\infty k^2H(k)\,\mathrm{d}k = -20\nu\int_0^\infty k^3F(k)\,\mathrm{d}k, \tag{2.35}$$

which is the spectral counterpart of (2.26).

In order to determine the approximate magnitude and shape of the function $a(r)$ for small r in an experimental situation, we keep the two leading-order terms in (2.24) and use the isotropic relations (2.25) and (2.31),

$$a(x) = -\frac{h}{6}x + \frac{\chi_h}{120\nu}x^3. \tag{2.36}$$

With this expression, a will have a minimum at $x = \sqrt{10\nu h/\chi_h}$, if $\Omega > 0$, as in a bottom Ekman boundary layer on the northern hemisphere. If, on the other hand, $\Omega < 0$, as in a corresponding Ekman layer on the southern hemisphere, a will have a maximum at the same location. With a helicity spectrum of the theoretical form,

$H(k) \sim \chi_h \epsilon^{-1/3} k^{-5/3}$, we can make the estimate $h/\chi_h \sim l_t^{2/3}\epsilon^{-1/3} \sim u_{rms}^2/\epsilon$, where we have used the standard estimate $l_t \sim u_{rms}^3/\epsilon$, for the turbulent integral length scale. Thus, the extreme point will be located around the Taylor microscale $\lambda = \sqrt{15\nu u_{rms}^2/\epsilon}$. As we will see in the following, $h \sim \epsilon/u_{rms}$ within the log layer, although there might be a logarithmic dependence with Re. The magnitude of the minimum/maximum can thus be estimated as $|a| \sim h\lambda \sim u_{rms}^2 Re_\lambda^{-1}$, where $Re_\lambda = u_{rms}\lambda/\nu$. In the atmospheric boundary layer we have $\lambda \sim 10$ cm, $u_{rms} \sim 1$ m s^{-1} and $R_\lambda \sim 10^4$ (Dhruva, Tsuji & Sreenivasan 1997). Thus, we would have $|a| \sim 10^{-4}$ m^2 s^{-2} and to measure the variation of a for small separation distances, we would need to measure velocities at least with an accuracy of 1 cm s^{-1} at length scales which are smaller than 10 cm. This is clearly feasible using hot wires (Dhruva *et al.* 1997). What seems more critical is that it may require a very long time to collect a sample which is large enough, in order to obtain a statistically converged result, since the correlation function $a(r)$ will come out as a rest after cancellations between high-amplitude positive and negative values. To make a fair estimate of the sampling time, a good intermittency model for the helicity would be required, which we do not have. We can only point out that the measurement by Koprov *et al.* (2005) suggests that it is possible to measure the mean turbulent helicity and that helicity spectrum with some degree of accuracy in an atmospheric boundary layer.

3. Analysis of a DNS

We have recently carried out high-resolution numerical simulations of the Ekman layer at moderately high Reynolds number $Re = G\delta_E/\nu$ (Deusebio *et al.* 2014). Here, G is the geostrophic wind far from the wall, ν the kinematic viscosity and $\delta_E = \sqrt{\nu/\Omega}$ the laminar Ekman boundary-layer thickness (Vallis 2006). The simulations have been carried out using a pseudo-spectral code based on Fourier series in the horizontal directions, x and z, and odd/even Chebyshev polynomials in the vertical direction y (Deusebio 2013). The velocity components along x, y and z are denoted by u, v and w, respectively. We use the no-slip condition at the wall, periodic boundary conditions in both horizontal directions and a stress-free condition at the top of the domain, that is $\partial_y u = \partial_y w = 0$ and $v = 0$ at the top of the domain. In this communication we analyse the helicity dynamics in the neutrally-stratified simulation at $Re = 1600$. This simulation produces a logarithmic region over roughly one decade and with a von Kármán constant similar to what was found in other wall-bounded flows (El Khoury *et al.* 2013). In figure 1(*a*) we plot the mean velocity profile, $\sqrt{\overline{u}^2 + \overline{w}^2}/u_\tau$, where $u_\tau = \sqrt{\tau_w/\rho}$ is the friction velocity and τ_w the wall shear stress. Figure 1(*b*) shows the odograph of the horizontal velocities, commonly referred to as Ekman spiral (see e.g. Vallis 2006). More details about the simulation can be found in Deusebio *et al.* (2014).

We start by considering the vertical profile of helicity. In the following data analysis, we will interpret the ensemble average $\overline{\cdot}$, used in §§ 2 and 2.2, as an average in time and over a horizontal plane. In figure 2(*a*), H, normalised by the magnitude of the local mean velocity and vorticity vectors, is shown. In the main part of the boundary layer H is positive (right-handed) and, at around $y^+ \approx 10^3$, it peaks with values very close to unity. At this height, the velocity profile also shows a maximum, usually referred to as the low-level jet (figure 1). Above $y^+ \approx 10^3$, H quickly decreases and attains negative values. A similar profile, positive close to the wall and negative in the upper part of the boundary layer, is also observed for the turbulent helicity h, shown in figure 2(*b*). One way to normalise the mean turbulent helicity would be to use $\omega_{rms}u_{rms}$.

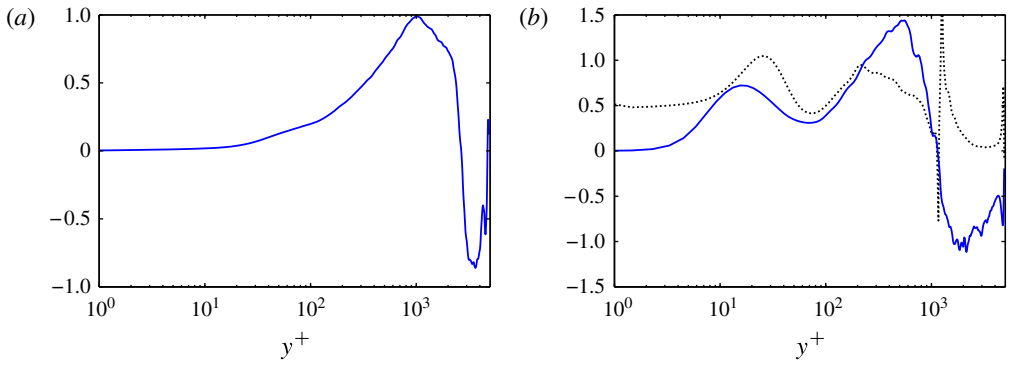

FIGURE 2. (Colour online) (*a*) Mean helicity profile $H/\,|\overline{u}|\,|\overline{\omega}|$ and (*b*) turbulent helicity profile $h\mathcal{K}^{1/2}/\varepsilon$. The dotted line indicates $h\varepsilon/\chi_h\mathcal{K} = hu_t/\chi_h l_t$; the singularity at $y \approx 10^3$ is due to a vanishing helicity dissipation χ_h.

However, this quantity increases with Reynolds number since $\omega_{rms} \sim \sqrt{\varepsilon/\nu}$. On the other hand, if the helicity spectrum is of the form $\sim k^{-5/3}$ mean turbulent helicity cannot depend on any small viscous length scale and should therefore stay finite in the limit of high Reynolds number. Therefore, we do not use a normalisation based on $u_{rms}\omega_{rms}$, but we rather use the local turbulent kinetic energy $\mathcal{K} = \overline{u_i' u_i'}/2$ and the turbulent kinetic energy dissipation $\varepsilon = \nu\overline{\partial u_i'/\partial x_k \partial u_i'/\partial x_k}$. We can thus form a turbulent length scale $l_t = \mathcal{K}^{3/2}/\varepsilon$ and a turbulent velocity scale $u_t = \sqrt{\mathcal{K}}$. We find that hl_t/u_t^2 attains values of the order of unity throughout the boundary layer. The profile of hl_t/u_t^2 has two peaks, with the inner peak located at $y^+ = 10$, a dip at around $y^+ \approx 10^2$ and a subsequent increase in the logarithmic region, between $10^2 < y^+ < 10^3$. The switch of sign of h ($y^+ \approx 6 \times 10^2$) is located somewhat closer to the wall as compared with H ($y^+ \approx 10^3$). That the mean field and turbulent helicity are generally positive in the lower part of the boundary layer and negative in the upper part is consistent with relation (2.16), which gives a positive/negative helicity injection in the lower/upper part of the boundary layer.

In figure 3 we show the different terms of the budget equation for H (figure 3*a*) and for h (figure 3*b–d*). In the inner region of the boundary layer the magnitude of the terms in the helicity budget equation can be estimated as in the laminar case, which is as $\sim G^2\nu/\delta_E^3 \sim u_\tau^4\Omega^{1/2}/\nu^{3/2}$. In the outer region the magnitude can be estimated as $\sim \Omega G^2/\delta \sim \Omega^2 G^2/u_\tau$, where we have used (2.16) and the estimate $\delta \sim u_\tau/\Omega$ for the turbulent Ekman boundary-layer thickness (Spalart *et al.* 2009; Deusebio *et al.* 2014). Close to the wall, the main balance in (2.3) is between I and the mean viscous dissipation χ_H. The term T accounts for a transport of positive helicity from larger y to the wall. Viscous diffusion of mean helicity (not shown), $\nu\nabla^2 H$, is large only very close to the wall. Positive mean helicity is transferred to turbulent helicity via P which peaks at around $y^+ = 10$. This is also the location at which the turbulent kinetic energy production attains its maximum (Deusebio *et al.* 2014). The turbulent helicity h is only forced by P which is mainly balanced by χ_h. In the inner region (figure 3*b*), two other terms also make a significant contribution: the transfer term t and the pressure transfer term i. In the logarithmic region (figure 3*c,d*), only the pressure transfer term i makes a significant contribution and it accounts for a transfer of helicity towards the wall where it is dissipated.

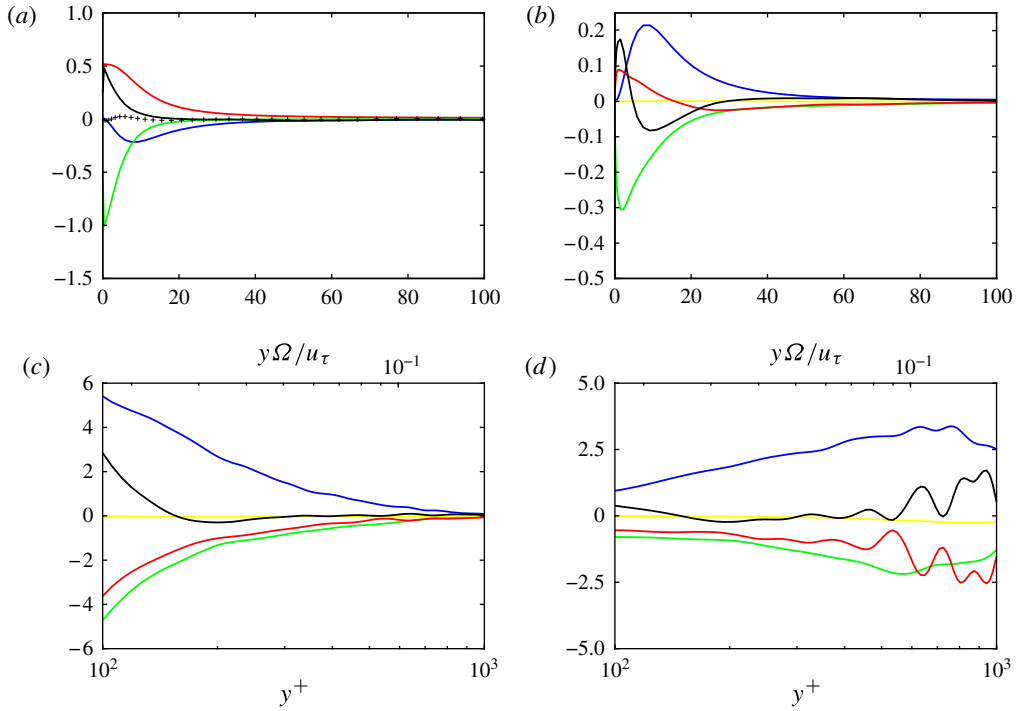

FIGURE 3. (*a*) Mean field helicity budget equation: blue, production P; red, pressure transfer I; green, viscous dissipation $-\chi_H$; black, transport term T. Here + sum of all of the terms of (2.3).*y*-axis scaled by $u_\tau^4/\nu^{3/2}\Omega^{1/2}$. (*b*) Turbulent helicity budget equation: blue, production P; green, viscous dissipation $-\chi_h$; yellow, Coriolis transport term r; black, transport term t; red, pressure transport term i, obtained as balance of the other terms. Here *y*-axis scaled by $u_\tau^4/\nu^{3/2}\Omega^{1/2}$. (*c*) Lines as in (*b*). Budget quantities are normalised by $\Omega^2 G^2/u_\tau$. (*d*) Lines as in (*b*). Budget quantities are normalised by $u_t^3/l_t^2 = \varepsilon^2/\mathcal{K}^{3/2}$. The vertical direction y is scaled with the viscous length, $y^+ = yu_\tau/\nu$ in all of the plots. (*c*,*d*) In the upper *x*-axis of the plots, the vertical direction is scaled with the outer scale $\delta = u_\tau/\Omega$.

It is worth pointing out that the only term which explicitly contains the rotation rate, r, is relatively small throughout the Ekman layer in the stationary state. Figure 3(*d*) shows a blow up of the logarithmic region in which the vertical axis was scaled by $u_t^3/l_t^2 = \varepsilon^2/\mathcal{K}^{3/2}$. The transport term t (and consequently i, which is derived as imbalance of the other terms in (2.4)) shows some wiggles as the outer region is approached which are likely to be due to a poor convergence for this term. Interestingly, P and χ_h attain values of the order of unity, suggesting that the helicity cascade is of comparable intensity as the energy cascade. If an approximate equilibrium of the helicity dynamics exists at each level, then (2.17) can be relaxed to be locally fulfilled. Close to the wall, the main balance is between I and χ_H; whereas in the outer, where the vertical mean gradients reduce, the main balance is between I and χ_h.

We will now test the isotropic relations derived in § 2.2. In practice, the two-point correlation $a(r)$ would be most easily measured by using Taylor's hypothesis with the separation vector aligned in the mean wind direction. However, in order to test the relations derived above as well as the degree of isotropy, $a(r)$ has been calculated

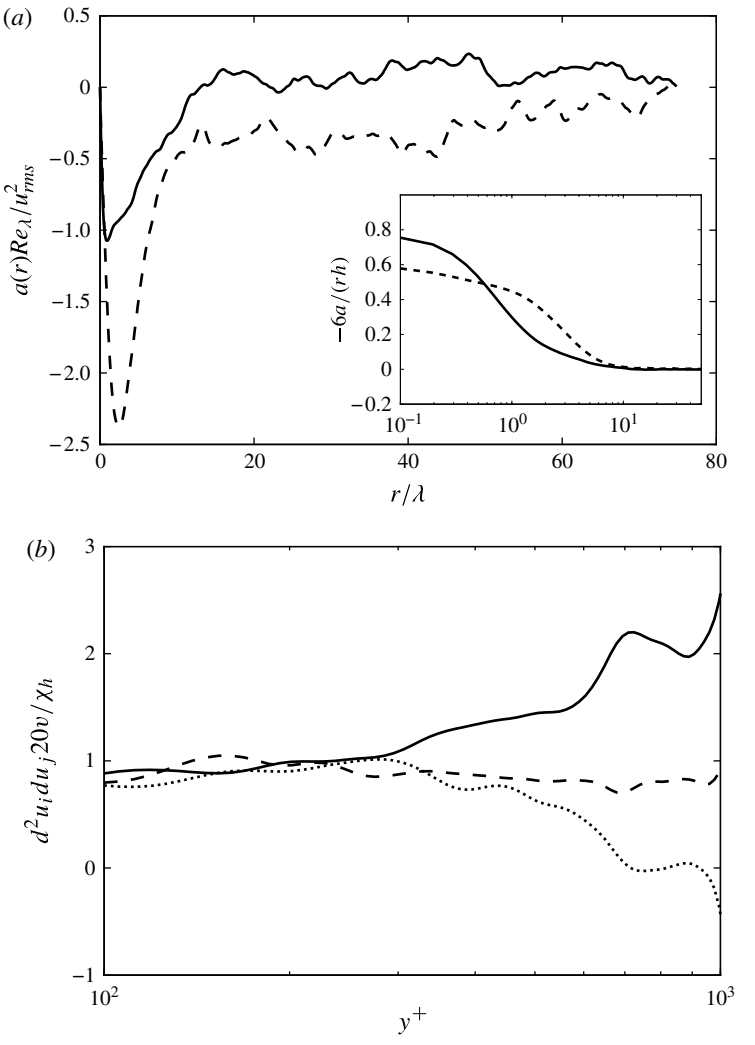

FIGURE 4. Validity of the isotropic relations derived in § 2.2. (*a*) Estimate of the turbulent helicity h using the $a(r)$ function: —— $a(r_x) = \overline{w'v - v'w}/2$; ---- $a(r_z) = \overline{v'u - u'v}/2$. (*b*) Estimate of the turbulent helicity dissipation χ using relation (2.26): —— $20\nu\,\overline{\partial_x^2 v \partial_x w}$; ---- $20\nu\,\overline{\partial_y^2 w \partial_y u}$; ..... $20\nu\,\overline{\partial_z^2 u \partial_z v}$.

directly in physical space along the x- and z-axis, respectively, at $y^+ \approx 200$, i.e. within the logarithmic region. At this vertical position we have $Re_\lambda = 260$. The two different curves representing $a(r)$, normalised by $u_{rms}^2 Re_\lambda^{-1}$, are shown in figure 4(*a*). Isotropy is clearly not fulfilled, since the two curves are quite different. However, both of them show a minimum around the Taylor microscale and the magnitude of the minima is around unity, as predicted in § 2.2. The inset in the figure shows $-6a(r)/r$ normalised by h, calculated using the two different expressions for $a(r)$. According to (2.36) both of the curves should approach unity in the limit of small r, if isotropy were to be fulfilled. As seen in the figure, both curves reach values which, although slightly smaller, are close to unity, thus providing general support to the relation (2.36).

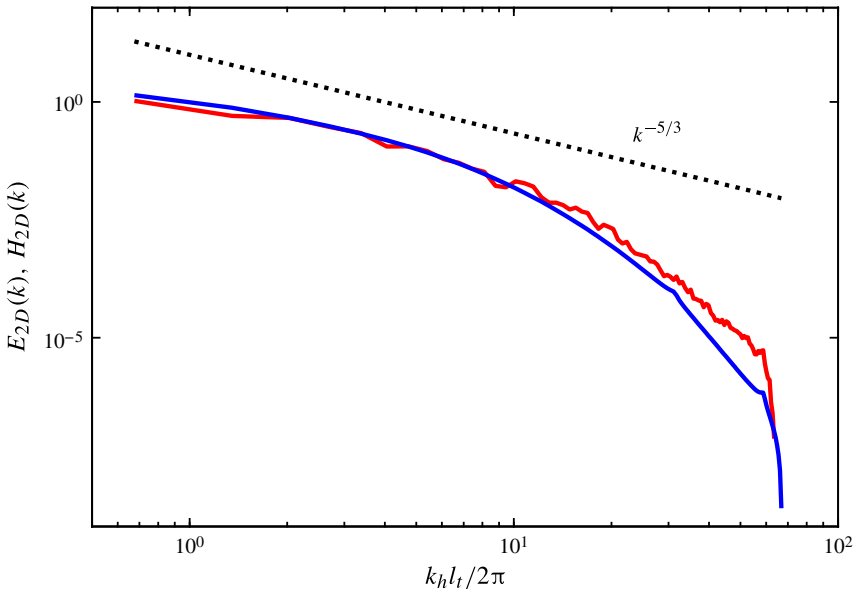

FIGURE 5. Blue, energy spectrum E_{2D}, given by (3.1*a*), and red, helicity spectrum H_{2D}, given by (3.1*b*), at $y^+ \approx 250$. The x axis is normalised by $2\pi/l_t$, with $l_t = \mathcal{K}^{3/2}/\varepsilon$. The energy spectrum is normalised by $\varepsilon^{2/3} l_t^{5/3}/(2\pi)^{5/3}$ and the helicity spectrum is normalised by $\varepsilon_h l_t^{5/3}/\varepsilon^{1/3}(2\pi)^{5/3}$. Dotted line: $10 \cdot (k_h l_t/2\pi)^{-5/3}$.

In figure 4(*b*), we test relations (2.26) which can be used in order to estimate the helicity dissipation χ_h. All three expressions have been calculated and compared for wall distances lying within the logarithmic region of the boundary layer. They all attain values very close to unity when scaled with the helicity dissipation χ_h. This is particularly true in the lower part of the logarithmic region. We can thus conclude that at the very smallest scales, comparable to the Kolmogorov scale, isotropy is fairly well satisfied. As the outer region is approached, $\partial_x^2 v \partial_x w$ and $\partial_z^2 u \partial_z v$ start to deviate significantly from unity, whereas $\partial_y^2 w \partial_y u$ continues to provide a good estimate of χ_h.

The two-dimensional energy and helicity spectra, H_{2D} and E_{2D}, are plotted in figure 5. They are not too far from showing a dependence of the form

$$E_{2D}(k_h) \sim C_E \varepsilon^{2/3} k_h^{-5/3} \quad \text{and} \quad H_{2D}(k_h) \sim C_H \varepsilon^{-1/3} \chi_h k_h^{-5/3} \qquad (3.1a,b)$$

in an intermediate wavenumber range, although a wider range would be needed to draw more definite conclusions. If we fit the spectra to $k^{-5/3}$ power laws in an intermediate range of wavenumbers we obtain the values $C_E = 1.6$ and $C_H = 1.4$ for the two constants, which are both of the order of unity, lending some support to the interpretation that the Reynolds number is just on the limit for a $k^{-5/3}$ scaling range to emerge. With energy and helicity spectra of the form (3.1) the turbulent mean helicity can be estimated as $h \sim \mathcal{K}\chi_h/\varepsilon$. Such a scaling is shown in figure 2(*b*), where $h\varepsilon/(\chi_h \mathcal{K})$ is plotted in dotted line and exhibits a plateau in the logarithmic region. At small wavenumbers both spectra, $E_{2D}(k_h)$ and $H_{2D}(k_h)$, flatten at large scale at about $k_h = 2\pi/l_t$, confirming the estimate $l_t \sim \mathcal{K}^{3/2}/\varepsilon$ (Batchelor 1953; Pope 2000) for the turbulent integral length scale.

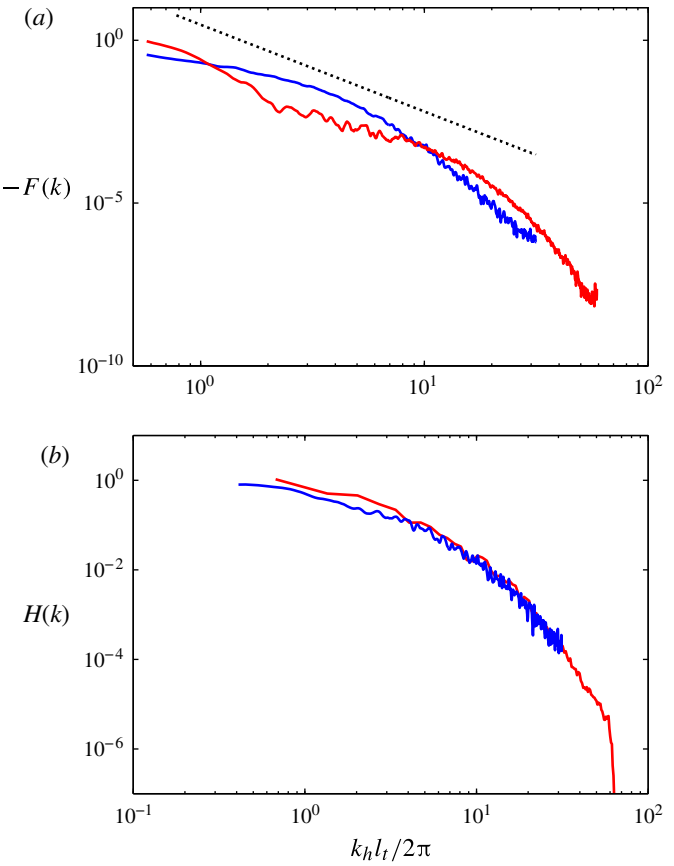

FIGURE 6. (*a*) Plot of $-F(k)$, relation (2.29), using (blue) $a(r_x) = \overline{w'v - v'w}/2$ and (red) $a(r_z) = \overline{v'u - u'v}/2$. Here $-F(k)$ is normalised by $\chi_h l_t^{8/3}/\varepsilon^{1/3}(2\pi)^{8/3}$. Helping line: $k^{-8/3}$. (*b*) Comparison of (red) the two-dimensional helicity spectrum $H(k)$ and (blue) its estimation based on $F(k)$, relations (2.30) and (2.34). Normalisation as in figure 5.

As shown in § 2.2, the form of the two-dimensional spectrum can also be estimated from the sine transform, $F(k)$, of $a(r)$. Figure 6(*a*) shows $-F(k)$ obtained from $a(r_x)$ and $a(r_z)$ at $y^+ \approx 250$. Although moderately noisy, the curves show a scaling not very far from $k^{-8/3}$ in an intermediate range of scales. However, in this range the two curves are quite separated from each other. So we may conclude that the Reynolds number is not sufficiently large for recovering isotropy at scales within the inertial range. The mean of the two curves has been used in order to estimate the two-dimensional spectrum, using relations (2.30) and (2.34), and the comparison with the actual helicity spectrum $H_{2D}(k)$ is shown in figure 6. A reasonable agreement is obtained, and the two spectra show very similar behaviour. Nevertheless, similar to what already observed in figure 4, the magnitude of $H_{2D}(k)$ is under-predicted by a factor of roughly 2 at small and intermediate wavenumbers, indicating that isotropy is not fulfilled in this range.

In figure 7, we plot the probability density function (p.d.f.) of the turbulent helicity at $y^+ \approx 250$. In spite of the positive bias observed (figure 2), the p.d.f. of $\boldsymbol{u}' \cdot \boldsymbol{\omega}'$ shows a quite symmetric shape with quite extended tails, both in the positive and

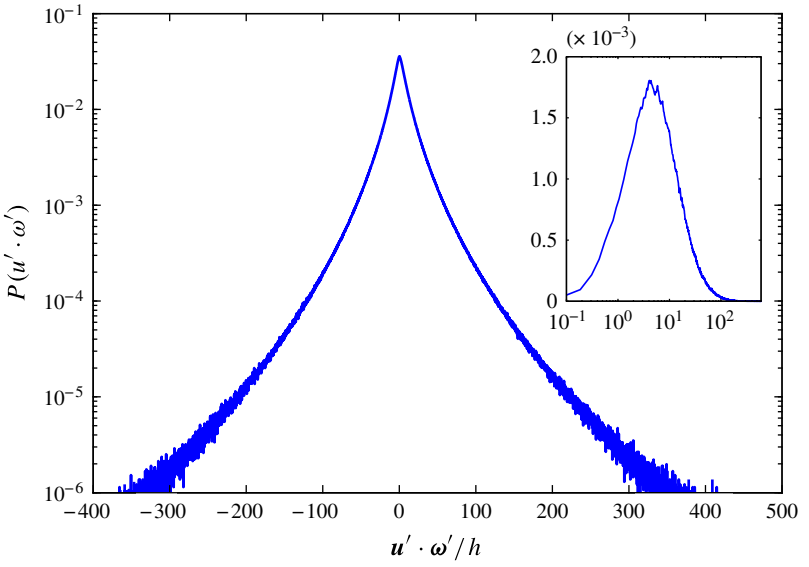

FIGURE 7. (Colour online) Probability density function (p.d.f.) of $\boldsymbol{u}' \cdot \boldsymbol{\omega}'$. Inset: Difference between the positive and negative tail of the p.d.f., $P(x) - P(-x)$.

negative directions, indicating that negative helicity appears in the flow with almost as high probability as positive helicity. In the inset of figure 7, we plot the difference between the positive and the negative tails of the p.d.f. The maximum of the difference appears at $\sim$10 h. We found a standard deviation σ of approximately $30\,\varepsilon/\mathcal{K}^{1/2}$, i.e. large compared with the mean value which is about unity (figure 2). The skewness is very small, approximately 3×10^{-3}, confirming the large degree of symmetry exhibited by the p.d.f. This is in agreement with results in helical homogeneous turbulence which show an almost symmetric p.d.f with a large cancellation between positive and negative helicity. Chen, Chen & Eyink (2003*a*) showed that the energy cascade leads to large values of helicity at small scales, which diverge in the limit of infinite *Re*.

In figure 8 we investigate to what degree the tails of the p.d.f. contribute to the mean helicity by considering the convergence of

$$\mathcal{F}(h_I) = \int_{-h_I}^{h_I} P(\zeta)\,\zeta\,\mathrm{d}\zeta \quad \text{with } \zeta = \boldsymbol{u}' \cdot \boldsymbol{\omega}', \tag{3.2}$$

to h as $h_I \to \infty$. It can be concluded from the figure that in order to measure h with a fair degree of accuracy, one would need to capture helicity events of very large intensity, in our case roughly 10^2 times larger than the mean helicity. As shown by the p.d.f. in figure 7, in our case such events have a probability of the order of 10^{-4}. We are faced with an apparent paradox here. Our results suggest that we really need to measure high-intensity events, which are in general associated with the small scales, in order to obtain an accurate estimate of h. On the other hand, this seems contradictory to the cascade theory and a helicity spectrum of the form of (3.1), according to which the main contribution to the mean helicity should come from scales of the order of l_t, at which mean helicity is also generated. By integrating (3.1) up to the wavenumber associated with the Taylor microscale, λ, the error on the estimate of h would be of the order of $(\lambda/l_t)^{2/3} \sim Re_\lambda^{-2/3}$, and therefore negligible in the atmospheric boundary

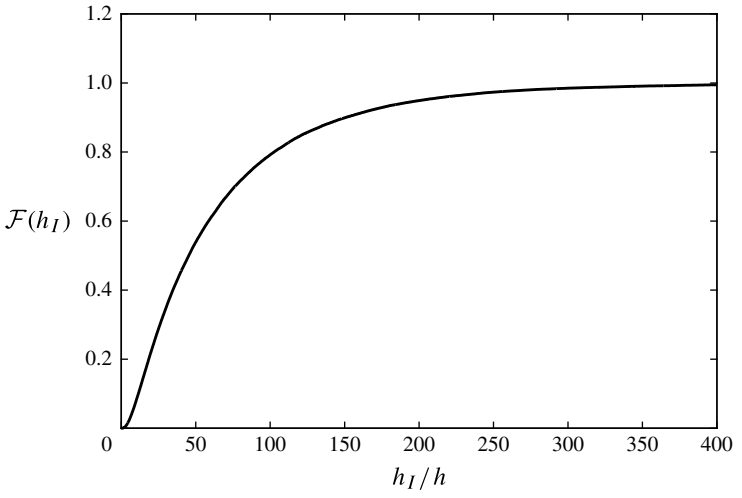

FIGURE 8. Convergence to the mean helicity content h as the tails of the p.d.f. are included.

layer where $Re_\lambda \approx 10^4$. This paradox could, of course, be resolved if the cascade theory were wrong. We find this unlikely. The most likely resolution of the paradox is that events of $|\boldsymbol{u}' \cdot \boldsymbol{\omega}'| \sim 100h$ do not exclusively correspond to very small scales, but have a significant contribution from large and intermediate scales. This part of the p.d.f. shall therefore be *Re*-independent. Indeed, the far-off tails of the p.d.f., i.e. events for which $|\boldsymbol{u}' \cdot \boldsymbol{\omega}'| \sim \epsilon^{3/4}/\nu^{1/4} \sim hRe_\lambda^{1/2}$, still depends on *Re*. These events can be much larger than $100h$, if the *Re* is large enough. Unfortunately, the limited *Re* number considered in the study does not allow us to offer on the apparent paradox more than this crude speculation, as $Re_\lambda^{1/2} \approx 10$. Numerical simulations nowadays do not allow for larger *Re* than what has been considered in this study, and therefore a reliable measure of intermittency can only rely on experiments and/or measurements.

4. Summary and conclusions

We have derived evolution equations for the mean field helicity and the mean turbulent helicity in an Ekman boundary layer and also derived some basic isotropic relations between the two-point velocity correlation function, $a(r)$, of two transverse velocity components, and the helicity correlation function as well as the helicity spectrum. The most important analytical results are that the integrated injection of right-handed helicity is equal to $2\Omega G^2$ over the total depth of the Ekman boundary layer, and that this injection can only be balanced by viscous dissipation. In the uppermost part of the Ekman layer, the helicity injection will, however, be of opposite sign as compared to the totally integrated injection, leading to a switch of sign of helicity in the outer part of the boundary layer. Nevertheless, in the major part of the turbulent Ekman boundary layer, including the logarithmic range, there will be a cascade from large to small scales of right-handed mean helicity if $\Omega > 0$ and left-handed mean helicity if $\Omega < 0$. Since helicity is a reflectionally antisymmetric and inviscidly conserved quantity which undergoes a cascade, it will preserve a signature of the system rotation all the way down to the Kolmogorov scale. By carrying out a measurement at millimetre scale of the helicity dissipation in the logarithmic range of

the atmospheric boundary layer, one would therefore be able to determine in which hemisphere the measurement is performed. In general, in a bottom Ekman boundary layer such a measurement would lead to a positive helicity dissipation in the northern hemisphere and a negative helicity dissipation in the southern hemisphere. The same quantity, measured at millimetre scale, would therefore show different signs in the two hemispheres. We find this result very fascinating. More theoretically, this indicates that reflectional invariance, unlike rotational invariance, is not a general property of small-scale high-Reynolds-number turbulence. The isotropic relations which we have derived provide a toolbox which can be used in order to test the cascade theory experimentally. In particular, our demonstration that the helicity spectrum can be determined from the correlation function $a(r)$ has opened a road to measurements of the helicity spectrum using hot wires.

Analysis of data from a DNS in the light of the helicity budget equations confirms the general conclusion that there is a cascade of right-handed helicity in the logarithmic range when $\Omega > 0$, although the Reynolds number is only on the limit for a $k^{-5/3}$-range to appear. In a substantial part of the logarithmic range, isotropy is fairly well satisfied at the Kolmogorov scale. At larger scales, however, isotropy is poorly satisfied, due to a rather low Reynolds number. The probability distribution of helicity, displays very broad tails and the mean helicity comes out as a net result after a strong cancellation between high-intensity negative and positive helicity events. This result poses interesting questions regarding the nature of the cascade and on the influence of small-scale dissipative events on the tail of the p.d.f. of helicity. Further investigations are needed to resolve the paradox of how large-helicity events, generally determined by small-scale dynamics, can affect the overall helicity content, which is mainly determined by the large scales.

Everything points to the conclusion that we have found a flow case with a stable and steady turbulent helicity cascade, whose sign and magnitude can be predicted from general analytical arguments. We hope that this communication will stimulate further measurements in the atmospheric boundary layer aimed at studying the joint cascade of energy and helicity at high *Re*.

Acknowledgements

The authors would like to thank Dr Cecilia Rorai who gave a talk which inspired this work. Computer time on the Ekman system was provided by Swedish National Infrastructure for Computing (SNIC) with a generous grant by the Knut and Alice Wallenberg (KAW) Foundation.

REFERENCES

BATCHELOR, G. K. 1953 *The Theory of Homogeneous Turbulence*. Cambridge University Press.

BIFERALE, L. 2003 Shell models of energy cascade in turbulence. *Annu. Rev. Fluid Mech.* **35** (1), 441–468.

BIFERALE, L., MUSACCHIO, S. & TOSCHI, F. 2012 Inverse energy cascade in three-dimensional isotropic turbulence. *Phys. Rev. Lett.* **108** (16), 164501.

BORUE, V. & ORSZAG, S. A. 1997 Spectra in helical three-dimensional homogeneous isotropic turbulence. *Phys. Rev.* E **55** (6), 7005–7009.

BRISSAUD, A., FRISCH, U., LEORAT, J., LESIEUR, M. & MAZURE, A. 1973 Helicity cascades in fully developed isotropic turbulence. *Phys. Fluids* **16**, 1366–1367.

CHEN, Q., CHEN, S. & EYINK, G. L. 2003*a* The joint cascade of energy and helicity in three-dimensional turbulence. *Phys. Fluids* **15**, 361–374.

CHEN, Q., CHEN, S., EYINK, G. L. & HOLM, D. D. 2003*b* Intermittency in the joint cascade of energy and helicity. *Phys. Rev. Lett.* **90** (21), 214503.

CHKHETIANI, O. G. 1996 On the third moments in helical turbulence. *J. Expl Theor. Phys. Lett.* **63** (10), 808–812.

DEUSEBIO, E. 2013 Numerical studies in rotating and stratified turbulence. PhD thesis, KTH, Mechanics, Linné Flow Center, FLOW.

DEUSEBIO, E., BRETHOUWER, G., SCHLATTER, P. & LINDBORG, E. 2014 A numerical study of the unstratified and stratified Ekman layer. *J. Fluid Mech.* **755**, 672–704.

DHRUVA, B., TSUJI, Y. & SREENIVASAN, K. R. 1997 Transverse structure functions in high-Reynolds-number turbulence. *Phys. Rev.* E **56**, R4928–R4930.

EL KHOURY, G., SCHLATTER, P., NOORANI, A., FISCHER, P. F., BRETHOUWER, G. & JOHANSSON, A. V. 2013 Direct numerical simulation of turbulent pipe flow at moderately high Reynolds numbers. *Flow Turbul. Combust.* **91**, 475–495.

ETLING, D. 1985 Some aspects of helicity in atmospheric flows. *Beitr. Phys. Atmos.* **58** (1), 88–100.

GOMEZ, T., POLITANO, H. & POUQUET, A. 2000 Exact relationship for third-order structure functions in helical flows. *Phys. Rev.* E **61** (5), 5321–5325.

KHOLMYANSKY, M., KIT, E., TEITEL, M. & TSINOBER, A. 1991 Some experimental results on velocity and vorticity measurements in turbulent grid flows with controlled sign of mean helicity. *Fluid Dyn. Res.* **7** (2), 65–75.

KOPROV, B. M., KOPROV, V. M., PONOMAREV, V. M. & CHKHETIANI, O. G. 2005 Experimental studies of turbulent helicity and its spectrum in the atmospheric boundary layer. *Dokl. Phys.* **50**, 419–422.

KRAICHNAN, R. H. 1967 Inertial ranges in two-dimensional turbulence. *Phys. Fluids* **10** (7), 1417–1423.

KURIEN, S. 2003 The reflection-antisymmetric counterpart of the Kármán–Howarth dynamical equation. *Physica* D*: Nonlinear Phenomena* **175** (3), 167–176.

LILLY, D. K. 1986 The structure, energetics and propagation of rotating convective storms. Part II: helicity and storm stabilization. *J. Atmos. Sci.* **43** (2), 126–140.

MININNI, P. D., ALEXAKIS, A. & POUQUET, A. 2006 Large-scale flow effects, energy transfer, and self-similarity on turbulence. *Phys. Rev.* E **74** (1), 016303.

MININNI, P. D. & POUQUET, A. 2009 Helicity cascades in rotating turbulence. *Phys. Rev.* E **79** (2), 026304.

MOFFATT, H. K. 1969 The degree of knottedness of tangled vortex lines. *J. Fluid Mech.* **35** (1), 117–129.

MOFFATT, H. K. 1981 Some developments in the theory of turbulence. *J. Fluid Mech.* **106**, 27–47.

MOFFATT, H. K. & TSINOBER, A. 1992 Helicity in laminar and turbulent flow. *Annu. Rev. Fluid Mech.* **24** (1), 281–312.

POPE, S. B. 2000 *Turbulent Flows*. Cambridge University Press.

SHINGAI, K. & KAWAMURA, H. 2004 A study of turbulence structure and large-scale motion in the Ekman layer through direct numerical simulations. *J. Turbul.* **5**, N13.

SPALART, P. R., COLEMAN, G. N. & JOHNSTONE, R. 2009 Retraction: direct numerical simulation of the Ekman layer: A step in Reynolds number, and cautious support for a log law with a shifted origin. *Phys. Fluids* **21** (10), 109901.

THOMPSON, R. 2005 Explanation of SPC severe weather parameters. Available at http://www.spc.noaa.gov/sfctest/help/sfcoa.html.

TSINOBER, A. & LEVICH, E. 1983 On the helical nature of three-dimensional coherent structures in turbulent flows. *Phys. Lett.* A **99** (6), 321–324.

VALLIS, G. K. 2006 *Atmospheric and Oceanic Fluid Dynamics: Fundamentals and Large-Scale Circulation; Electronic Version*. Cambridge University Press.

ZHEMIN, T. & RONGSHENG, W. 1994 Helicity dynamics of atmospheric flow. *Adv. Atmos. Sci.* **11** (2), 175–188.